Thermographic nondestructive evaluation: overview of recent progress

C. Ibarra-Castanedo, F. Galmiche, A. Darabi, M. Pilla, M. Klein, A. Ziadi, S. Vallerand, J.-F. Pelletier, X. Maldague*

Computer Vision and Systems Laboratory, Dept. of Electrical and Computer Engineering
Université Laval, Quebec City, Canada. G1K 7P4

ABSTRACT

This paper presents a summary of recent research activities carried out at our laboratory in the field of Infrared Thermography for Nondestructive Evaluation (TNDE). First, we explore the latest developments in signal improvement. We describe three approaches: multiple pulse stimulation [1]; the use of Synthetic Data for de-noising of the signal [2]; and a new approach derived from the Fourier diffusion equation called the Differentiated Absolute Contrast method (DAC) [3]. Secondly, we examine the advances carried out in inverse solutions. We describe the use of the Wavelet Transform [4] to manage pulsed thermographic data, and we present a summary on Neural Networks for TNDE [5]. Finally, we look at the problem of complex geometry inspection. In this case, due to surface shape, heat variations might be incorrectly identified as flaws. We describe the Shape-from-Heating approach [6] and we propose some potential research avenues to deal with this problem.

Keywords: Thermal Pulse Shaping, Synthetic Data, Differentiated Absolute contrast method, Pulsed Phase Thermography, Fourier Transform, Wavelet Transform, Neural Networks, Complex Shape Inspection.

INTRODUCTION

Thermography for Nondestructive Evaluation (TNDE) is a non-invasive and fast inspection technique with the capability to perform remote inspections on large surfaces. These features give thermography an interesting advantage with respect to other NDE approaches [7]. Nevertheless, TNDE faces several problems that complicate the detection and characterization of defects: emissivity problems, non-even heat distribution, and surface shape. We present here a review of different thermographic techniques that have shown promising results.

In the first section of this paper we explore three novel techniques for signal improvement. We begin our discussion with the "multiple pulse stimulation" approach, where the idea is to "shape" the thermal pulse to optimize the spectral frequency distribution improving defect visibility. Next, we explore the use of synthetic data for signal de-noising. Other than de-noising, synthetic data confers the possibility to work with analytical solutions and may be used for data reduction. We then present the Differentiated Absolute Contrast method (DAC) [3] that has proven effective to manage non-uniform heating eliminating at the same time the need of a sound area definition used by classical contrast methods.

Section 2 describes the advances accomplished to solve the inverse problem. First, we recall the basic theory behind Pulsed Phase Thermography (PPT) [8] using the Fourier Transform (FT). PPT has been successfully used for defect detection applications. However, given the noisy and non-linear nature of pulsed thermographic data, inverse solutions are difficult to achieve. An approach using the Wavelet Transform (WT) instead of the FT was proposed [4]. Unlike the FT, the WT preserves the time information of the signal, which is correlated to the defect depth, allowing quantitative evaluations. Neural Networks (NN) are also reviewed. NN are powerful, robust and adaptive tools for detecting and classifying. It is not a surprise that NN were introduced recently for TNDE applications. We present here a summary of the latest achievements on the subject.

* Corresponding author. Tel.: + 1-418-656-2962; fax: + 1-418-656-3594, Email address: maldagx@gel.ulaval.ca

In section 3, we analyze the complex shape problem. We describe the parameters involved when a non-planar object is inspected by TNDE, we summarize the different techniques that have been developed and we provide some insight on future research.

1. SIGNAL IMPROVEMENT

1.1. Multiple pulse stimulation

The stimulation of a specimen with two consecutive pulses was recently proposed [1]. To explain this concept we refer to Figure 1, where two situations are considered. The first possibility consists to stimulate the specimen with a unique Δ duration pulse with an amplitude $2A$. The second case is the stimulation of the sample by two Δ duration consecutive pulses of amplitude A separated by δ. Total energy delivered to the specimen is exactly the same and equals $2A\Delta$. The corresponding frequency spectra is shown on Figure 1b. The difference is on the high frequencies. For the 2 pulse spectrum these are much more attenuated and therefore, noise is reduced and consequently subsurface structure visibility is increased.

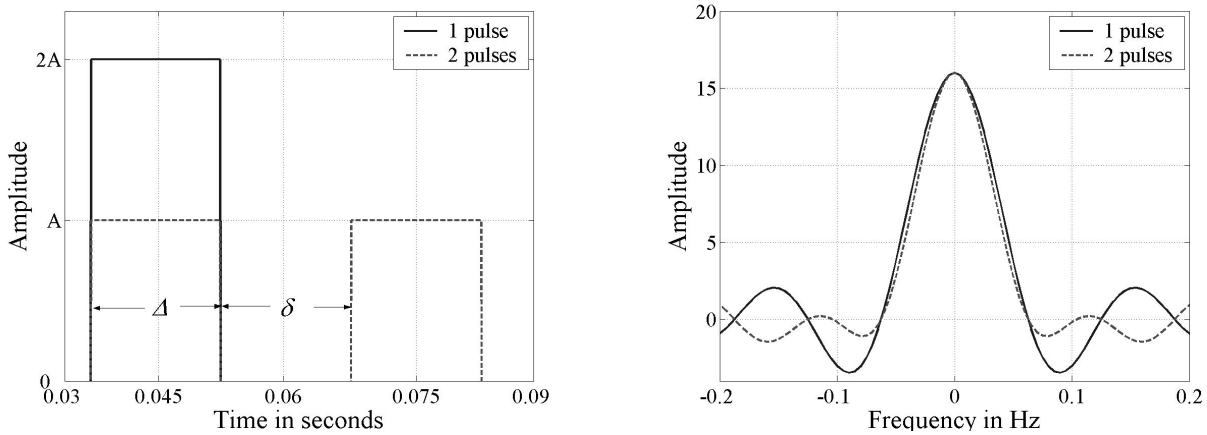

Figure 1. (a) Amplitude and (b) frequency spectrum distribution for the case of one Δ duration pulse of amplitude $2A$ (plain line); and 2 pulses of A amplitude separated by δ (dotted line).

For small δ values (δ~0), heat pulse is in fact enlarged and no signal improvement is expected. On the other hand, for δ values, enlarged up to a situation where the second pulse could be considered as repetition of the experiment, a reduction of visibility is in fact be observed. Therefore, the optimal value is in between these two limiting cases. Moreover, based on experimental results it was found that the separation interval δ between pulses was related to the material been inspected: high conductivity materials showed much lower optimal δ values with respect to low conductivity materials. Figure 8 illustrates this approach where phase images at 1.25 Hz are presented in a mild steel specimen with four flat-bottom holes from 1 to 3.5 mm depth as indicated. For this case δ=3 ms. Defect visibility is better for the 2 pulse case. Intensity profiles at the center of the defects are also included (Figure 8b). It can be seen from these profiles that the 2 pulse case shows a better contrast with respect to the 1 pulse situation.

1.2. Synthetic Data

Figure 2 shows schematically the heat diffusion model for a semi-infinite plate with a subsurface defect and the corresponding temperature evolution. After the pulse has reached the sample surface, heat propagation through the material is actually performed in a three-dimensional manner given by the Fourier diffusion equation:

$$\nabla^2 T - \frac{1}{\alpha}\frac{\partial T}{\partial t} = 0 \tag{1}$$

Several assumptions may be used to simplify equation (1). Carslaw and Jaeger [9] for example, proposed a one-dimensional solution for the case of a Dirac pulse applied on a semi-infinite plate without flaws:

$$\Delta T = \frac{Q}{e\sqrt{\pi t}} \tag{2}$$

or, in the logarithmic domain:

$$\ln T = \ln\left(\frac{Q}{e}\right) - \frac{1}{2}\ln(\pi t) \tag{3}$$

where ΔT is the temperature decrease on the surface, Q is the energy absorbed by the plate, t the time, and $e=(k\rho C)^{1/2}$ is the thermal effusivity, with k being the thermal conductivity, ρ the mass density and C the specific heat.

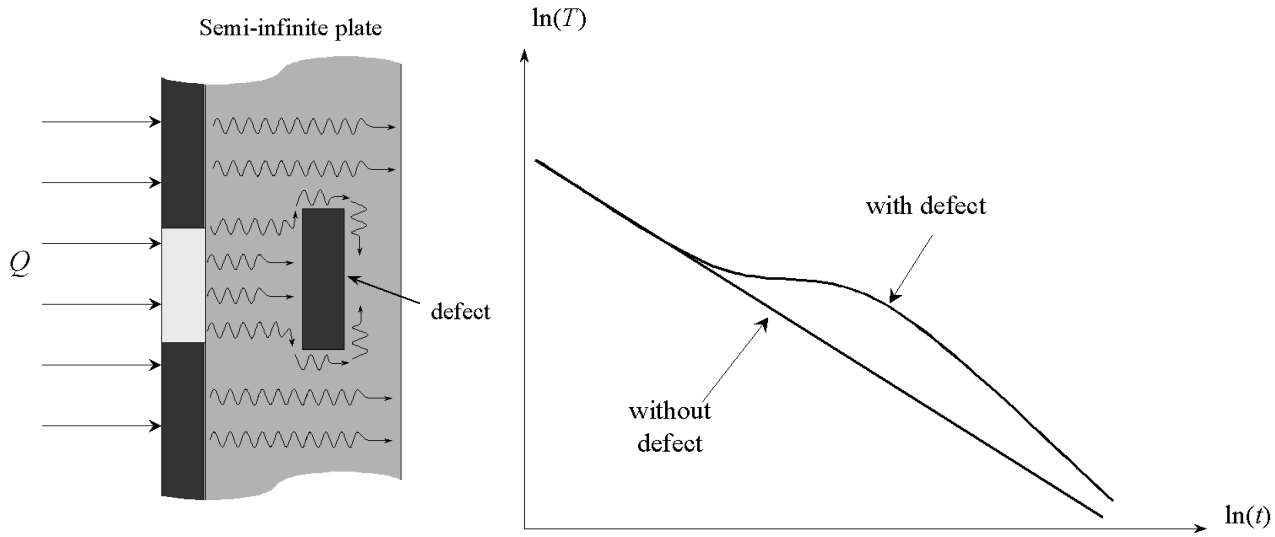

Figure 2. Heat diffusion model for a semi-infinite plate with a subsurface defect and the corresponding temperature evolution profiles after a heat pulse.

Before the heat wave reaches the defect, temperature decay is linear with a slope equal to –1/2 as predicted by equation (3). In the presence of a flaw however, heat propagation is no longer linear as seen on Figure 2. A two-dimensional solution would be more appropriate in this case:

$$\nabla^2_{x,y} T - \frac{1}{\alpha}\frac{\partial T}{\partial t} = 0 \tag{4}$$

To exploit the discrepancy on the temperature profile behavior between the plate and the defect, Shepard [10] proposed to fit the temperature decay curve to a polynomial:

$$\ln[T(t)] = a_0 + a_1 \ln(t) + a_2 \ln^2(t) + ... + a_n \ln^n(t) \tag{5}$$

Such procedure brings at least three advantages: substantial reduction on data to process, possibility to work with analytical solutions, and de-noising of high frequencies. To give an idea of these advantages we compare the raw coefficient image for coefficient a_0 of a 4th degree polynomial to the images obtained by Pulsed Phase Thermography (PPT) both to raw thermographic data, and to synthetic data. The results are shown on Figure 3.

Intensity profiles across the center of the defects are also included on Figure 3. This gives rise to some interesting observations. First, de-noising related to the fitting procedure is clearly seen by comparing direct and synthetic PPT, Figure 3c and Figure 3d, respectively. It is also noticed, that the use of the raw coefficient images are already interesting to internally resolve the structure of the specimen as seen on Figure 3b.

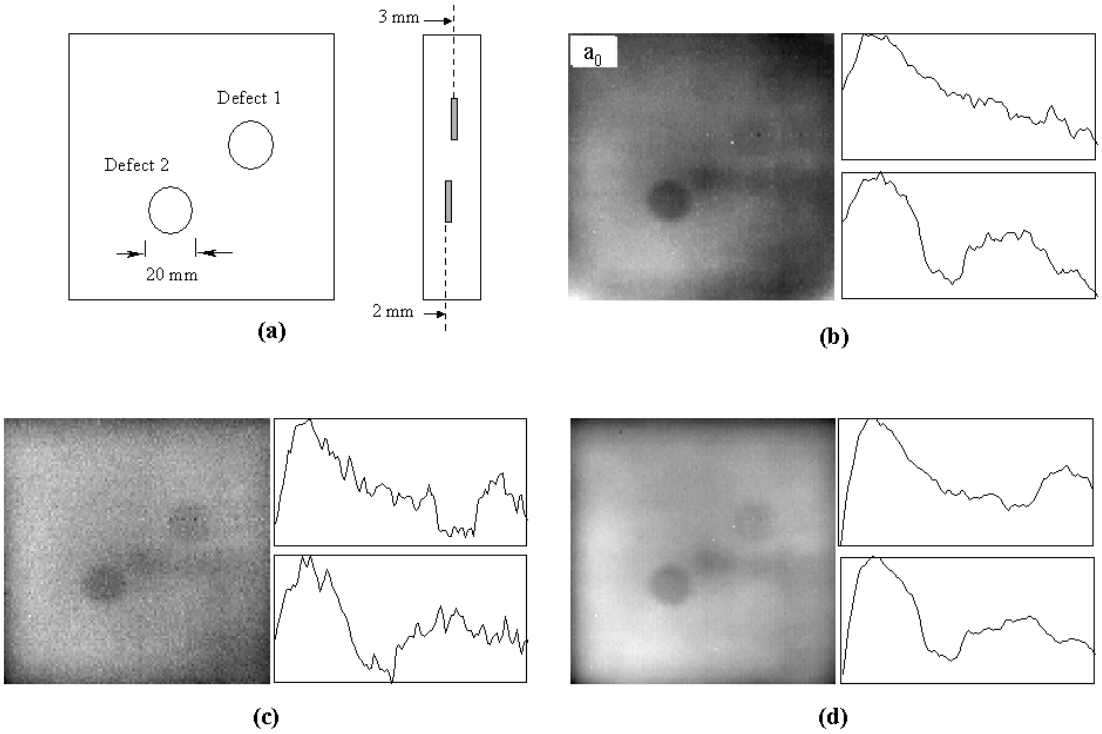

Figure 3. (a) Graphite epoxy plate 4 mm thick with 2 artificial Teflon® inclusions, 20 mm diameter, 2 (top) and 3 (bottom) mm depth; (b) raw coefficient a_0 image; (c) PPT, f=0.33 Hz; and (d) synthetic PPT, f=0.33 Hz. From [2].

1.3. Differentiated Absolute Contrast method (DAC)

Traditionally, contrast methods require the use of the temperature of a *sound* area (T_s) where it is known that no defect is present under the surface. Several definitions have been proposed to make contrast computations, the simpler one is the absolute contrast C_a defined as:

$$C_a(i,j,t) = T_{def}(i,j,t) - T_s(i,j,t) \tag{6}$$

where (i,j,t) are the coordinates at time of interest t, and T_{def} is the temperature of a point (i,j), which is know to be located on an area with a defect.

Contrast methods suffer from two major problems, first the definition of a sound area is not always practical or possible for most industrial applications, and second, the resulting data is strongly affected by non-uniform heating, a problem that is always present at some degrees in TNDE. The Differentiated Absolute Contrast method (DAC) had proven effective for managing non-even heating while making local contrast computations. Subjective defect-free-zone definition is no longer necessary. DAC equation is derived from the one-dimensional model of the Fourier equation after an instantaneous Dirac heating pulse is applied, equation (2). Derivation of the DAC equation is well documented in [3], here we present the final result:

$$C_{DAC}(i,j,t) = \Delta T(i,j,t) - \sqrt{\frac{t'}{t}}\Delta T(i,j,t') \tag{7}$$

where t' is a given value of time ranging from a reference time t_{ref} (see Figure 4 below), and the time at which the first defect becomes visible t_{def}.

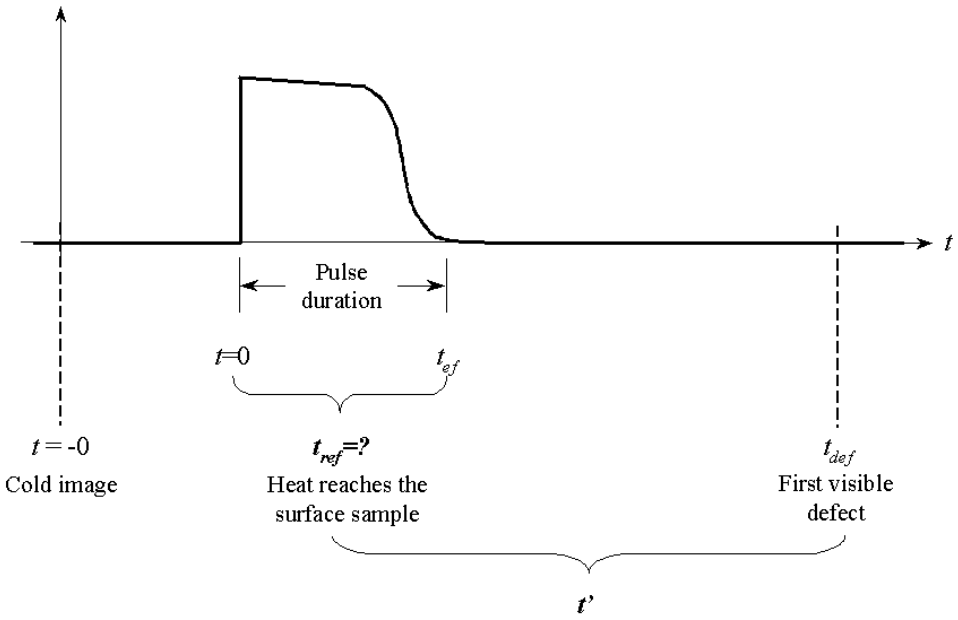

Figure 4. Heat pulse profile for a flash showing a slow return to zero at the end.
The different times involved on DAC computations are also shown.

An appropriate reference time t_{ref}, would be the instant at which heat reaches the surface sample. Nevertheless, as shown on Figure 4, this is not known accurately as the heat pulse approximates a square pulse instead of a Dirac pulse assumed in the derivation of equation (2). We can reasonably assume though, that t_{ref} is comprised between the beginning and the end of the pulse ($t=0< t_{ref}< t_{ef}$). In addition, heat pulse is generally short compared to the recording time; heat pulse can then be modeled by an instantaneous Dirac pulse, which, for instance gives rise to equation (7). The uncertainty associated with the estimation of t_{ref} forces us to compensate manually or automatically for the error as explained in [3].

DAC has proven effective against non-uniform heating as is shown on Figure 9. Figure 9a shows the raw thermogram of a typical sample of Plexiglas™. The corresponding 3D view is seen in Figure 9b. It is evident from these figures that the sample was subjected to a strong non-even heating as seen on the sharp variation of background intensity values. Figure 9c and d, show the thermogram and its 3D view, respectively, after the application of the DAC method. The effect of non-even heating is practically eliminated and defects are still visible with excellent contrast.

2. INVERSE SOLUTIONS

2.1. Pulsed Phase Themography (PPT)

Pulsed Phase Thermography (PPT) [8] is a well-documented technique (see Chapter 10 in [7]) that links Pulsed Thermography (operating in the transient regime) to Lock-in Thermography (operating in the stationary regime). The Fourier Transform (FT) is used to extract the various frequencies in PPT. The FT is expressed as:

$$F_n = \sum_{n=1}^{N} T(k) e^{2\pi j k n/N} = \mathrm{Re}_n + \mathrm{Im}_n \tag{8}$$

where j is an imaginary number, n designates the frequency increment, N is the total number of thermograms, and Re and Im are respectively the real and the imaginary parts of the transform. Amplitude A and phase ϕ data are available as follow:

$$A = \sqrt{\mathrm{Re}_n^2 + \mathrm{Im}_n^2} \qquad \phi = \tan^{-1}\left(\frac{\mathrm{Im}_n}{\mathrm{Re}_n}\right) \tag{9}$$

PPT using the FT has been successfully applied for defect detection. Some efforts was carried out with the objective to use pulsed thermographic data on inverse problems, Neural Networks for instance which are the subject of a subsequent section. The following section reviews an alternative approach to manage PPT data using Wavelets.

2.2. Wavelet Tranform (WT)

The Wavelet Transform (WT) may be used with PPT data in a similar manner as the FT, with one interesting advantage: wavelets preserve the time information of the signal (lost in the FT) and is correlated to the defect depth, allowing quantitative evaluations [4]. Using the WT, the signal *T(k)* for a pixel *(i,j)* is decomposed into stretched and scale replicas of the base wavelet. Two parameters become available: the translation factor *Tr*, and the scaling factor *S*:

$$W_f(S,T) = \int_{-\infty}^{+\infty} f(t) h^*_{ST_r}(t)dt = \mathrm{Re} + j\,\mathrm{Im} \tag{10}$$

where W_f denotes the WT, *f(t)* is the analyzed function and h_{STr} is the daughter wavelet defined from the mother wavelet:

$$h_{ST_r}(t) = \frac{1}{\sqrt{S}} h\left(\frac{t-T}{S}\right) \tag{11}$$

The mother wavelet used here is the Morlet wavelet defined as:

$$h(t) = e^{(j\omega_0 t)} e^{\left(-t^2/2\right)} \tag{12}$$

where ω_0 provides the size of the Morlet wavelet. Both real and imaginary parts become available, as seen on equation (10), so that phase and amplitude images can be computed as in the case of the FT. Using phase images, calibration of T_r provides a direct inversion of the defect depth for a given *S*.

Figure 10 illustrates this approach. It shows the phase values of the WT for a (a) 1 mm and (b) 3 mm depth defects (flat-bottom holes in aluminum) as a function of T_r for a line passing over the defect center. The defects are clearly visible.

2.3. Neural Networks (NN)

The purpose of this section is not to provide a detailed description of NN, which is for instance available elsewhere [5]. Here, we provide some insights on the subject as a result of several studies carried out in our laboratory.

NN was applied for defect detection (defect/no-defect) and for quantification (*i.g.* depth estimation). The results of these studies revealed that multi-layer Perceptron Neural Networks (PNN) achieve much better detection results than for instance Kohonen architectures (KNN) [11]. This is due to the limited quantity of information KNN are able to store with the limited number of neurons and adjustable weights used in these studies. Different kinds of data have been analyzed: raw temperature, contrast data, phase and amplitude. Moreover, phase data has shown limited sensitivity to noise and requires sufficiently high sampling rate with respect to thermal properties of the sample. Other strategies could be tried like the coupling of information using different kinds of data (*i.g.* using phase data for detection and amplitude data for characterization). Simulated data is privileged to experimental data during the training phase to avoid the use of redundant and non-representative information during training and to study noise effects on NN [5]. Figure 5 shows some results obtained with a PNN for a sample simulating corrosion on aluminum for: (a) temperature data, (b) amplitude data, and (c) phase data [11].

On one of the latest developments, a neuro-fuzzy depth estimator based on Adaptive-Network-based Fuzzy Inference System (ANFIS) modeling has been investigated [12]. The ANFIS system was tested with simulated and real data showing both accuracy and short training time on inversion TNDT problems thus providing better results as compared with NN based-depth estimators. However neuro-fuzzy depth estimators are more noise sensitive.

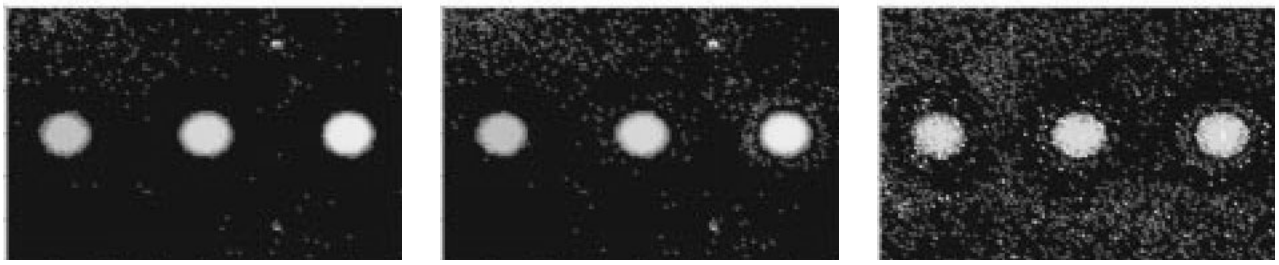

(a) **(b)** **(c)**

Figure 5. Results obtained with a PNN for a sample simulating corrosion on aluminum: (a) temperature data, (b) amplitude data, and (c) phase data. From [11].

3. COMPLEX GEOMETRY INSPECTION

3.1. The shape problem

TNDT techniques are usually used under the assumption that the part being inspected has a planar surface. However, when complex shape objects are examined, the surface geometry produces a signal distortion that may lead to faulty defect detection. Heat emission (as well as heat absorption) is at its maximum when the normal to the surface is parallel to the direction of the flow of energy (see Figure 6). Therefore, the emitted (or absorbed) signal is weaker when there is an angle between the normal on the surface and the direction of flow. This intensity reduction is caused exclusively by the surface geometrical variations but it can lead to incorrect subsurface defect detection if corrective measures are not adopted. Moreover, the points furthest away from the source (or sensor) will absorb (or will emit) less energy compared to the closer ones. In reference to Figure 6, in addition to the angle between the normal at the point B and the direction of flow, point B is located further from the source (and from the sensor) in comparison to point A. Without shape information on the object, defects located under the surface just below point B will be difficult to detect by TNDT.

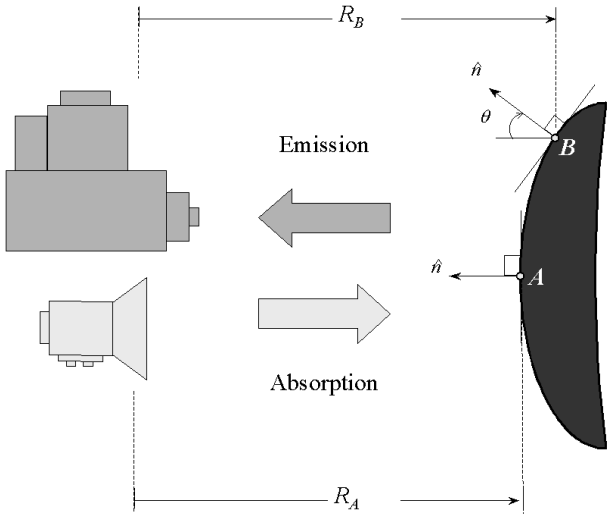

Figure 6. Complex shape inspection problem: the distance R, between the captor and the specimen, as well as the angle θ, between the normal and the direction of flow, contribute to the distortion of the thermographic data.

3.2. Shape-from-Heating (SfH)

Several techniques have been proposed to manage the complex shape problem [7]: point source heating, video thermal stereovision, direct calibration, and Shape-from-Heating (SfH). SfH stands out among other shape correction TNDE techniques because, besides the traditional TNDT apparatus, no additional equipment is needed. Furthermore, calibration steps are not mandatory. SfH is based on Shape-from-Shading theory [13] from the machine vision field although substantially modified for TNDT applications. Geometric extraction by SfH is made from the Early Recorded

Thermogram (ERT), *i.e.* the first (useful) thermal image of the sequence in which defect contrasts have not yet developed. Intensity variations are therefore exclusively related to surface geometry and not to the presence of a flaw. This allows shape extraction and the subsequent geometry correction of the entire thermogram sequence. Once shape correction is performed, thermograms may be treated as planar surfaces and traditional detection and quantification procedures may be used. SfH is carried out in three steps [6]: (1) ERT segmentation, (2) geometry extraction and (3) shape correction.

Figure 7 illustrates an example. Figure 7a and b, show the ERT and the segmented thermogram, respectively. Figure 7c, shows the surface geometry to be extracted from the sequence. Finally, on Figure 7d, the subsurface defect is detected as it would be for a planar surface.

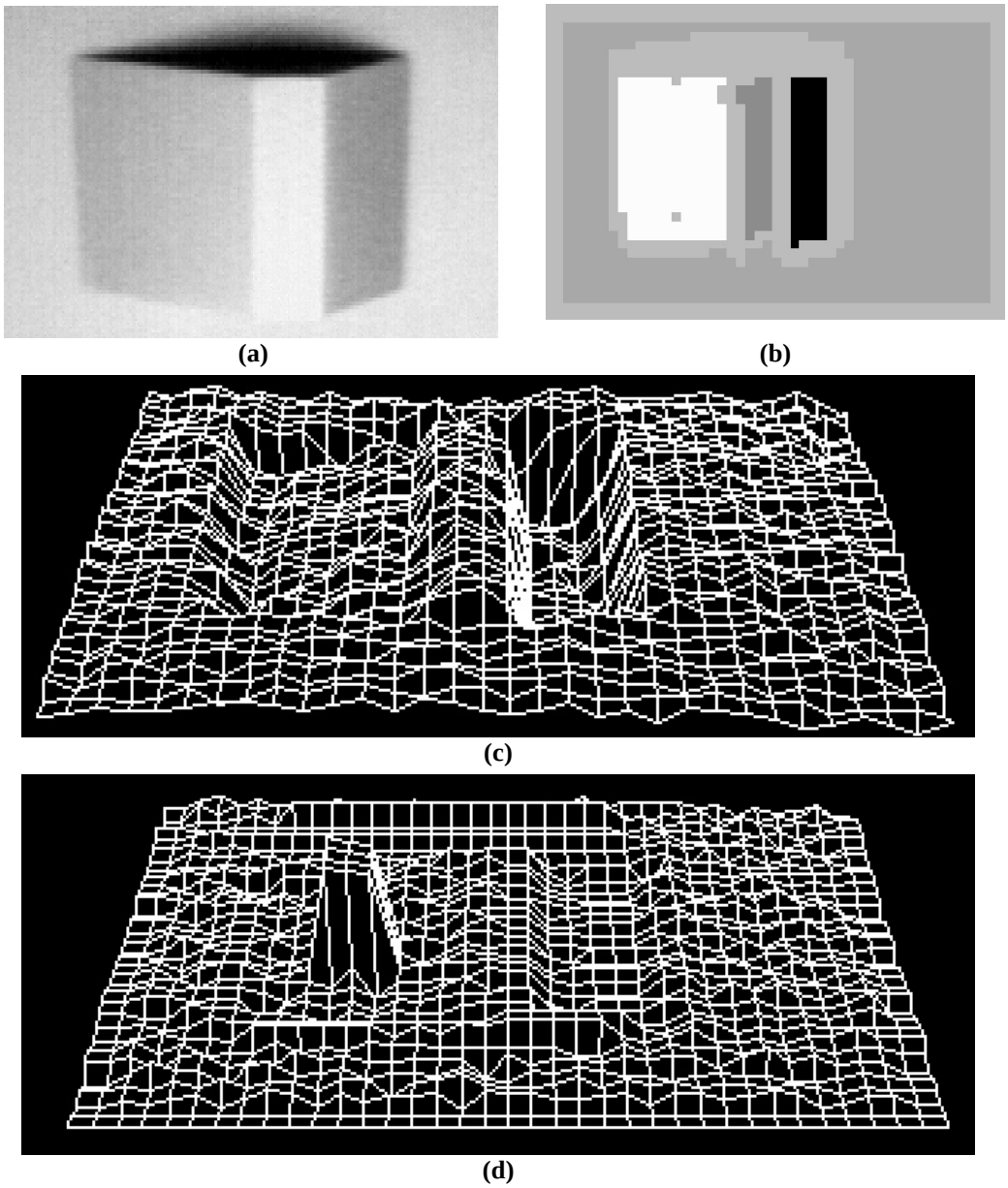

Figure 7. Shape from Heating (SfH) example. (a) Early Recorded Thermogram (ERT), (b) segmented thermogram, (c) shape extraction, and (d) defect detection seen on left. From [14].

3.3. Future work

There are still some difficulties that must be addressed to fully exploit the potential of SfH. First, SfH uses two different models for linear and non-linear surface areas. Transition between these two cases it not always smooth. A unique model is required. Signal noise is still a problem. The latest developments in signal improvement may help to propose better solutions.

CONCLUSIONS

In this paper, we presented a set of recent techniques to process thermographic data. Multiple pulse stimulation, synthetic data and DAC have shown promising results for signal improvement. In the text, we described these approaches along with some selected results. The inversion problem was also addressed. We presented the basic concepts of Wavelets and we summarized the state-of-the-art on Neural Networks for TNDE. Both approaches have shown great potential for defect characterization problems. Finally, the complex geometry problem was described. We examined the Shape-from-Heating technique and presented some results. Finally, we gave some insight about future work in this field.

REFERENCES

[1] 1. Maldague X.P, Galmiche F.and Ziadi A. “Advances in Pulsed Phase Thermography”, *Infrared Physics & Technology*, **43**: 175-181, 2002.

[2] 2. Ibarra-Castanedo C., Galmiche F. and Maldague X.P. “On Synthetic Data in Infrared Thermography for NonDestructive Evaluation”, *Canadian Association of Physicists Congress (CAP)*, Quebec, Canada, June 2 - 5, 2002.

[3] 3. Pilla M., Klein M., Maldague X. and Salerno A., “New Absolute Contrast for Pulsed Thermography,” in D. Balageas, G. Busse, C. Carlomagno ed.: *Proc. QIRT 2002 (Quantitative Infrared Thermography)*, Dubrovnik, Croatia, 2002.

[4] 4. Galmiche F. and Maldague X. “Depth defect retrieval using the wavelet pulsed phased thermography,” in D. Balageas, G. Busse, C. Carlomagno ed.: *Proc. QIRT 2000 (Quantitative Infrared Thermography)*, Eurotherm Seminar 64, Reims, France, pp. 194-199, 2000.

[5] 5. Darabi A. and Maldague X. “Neural Networks Based Detection and Depth Estimation in TNDE,” *Nondestructive Testing and Evaluation International*, **35**(3): 165-175, 2002.

[6] 6. Pelletier J-F. and Maldague X. “Shape-from-Heating : A Two-Dimensional Approach for Shape Extraction in Infrared Images”, *Opt. Eng.*, **36**(2): 370-375, 1997.

[7] 7. Maldague X.P. “Theory and practice of infrared technology for nondestructive testing”, John Wiley & Sons, N.Y., 2001.

[8] 8. Maldague X.P. and Marinetti S. “Pulse Phase Infrared Thermography”, *J. Appl. Phys.*, **79**(5): 2694-2698, 1996.

[9] 9. Carslaw H.S. and Jaeger J.C. “Conduction of Heat in Solids”. Clarendon Press, Oxford, 1959.

[10] 10. Shepard S.M. “Advances in Pulsed Thermography”, in A.E. Rozlosnik, R.B. Dinwiddie ed.: *Thermosense XXIII, Proc. SPIE (Society of Photo-Optical Instrumentation Engineers)*, **4360**: 511-515, 2001.

[11] 11. Vallerand S. and Maldague X. “Defect Characterization in Pulsed Thermography: A Statistical Method Compared with Kohonen and Perceptron Neural Networks”, *Nondestructive Testing and Evaluation International*, **33**(5): 307-315, 2000.

[12] 12. Darabi A. “Detection and estimation of defect depth in infrared thermography using artificial neural networks and fuzzy logic”, *Ph. D. thesis*, Université Laval, 2000.

[13] 13. Horn B. and Brooks M. “Shape from Shading”, MIT Press, Cambridge, MA, 1989.

[14] 14. Pelletier J-F. and Maldague X. “Infrared Thermography: Nonplanar Inspection”, in J.J. Burleigh, J.W Spicer. ed.: *Proc. SPIE: Thermosense XVIII*, **2766**(March): 264-275, 1996.

COLOR FIGURES

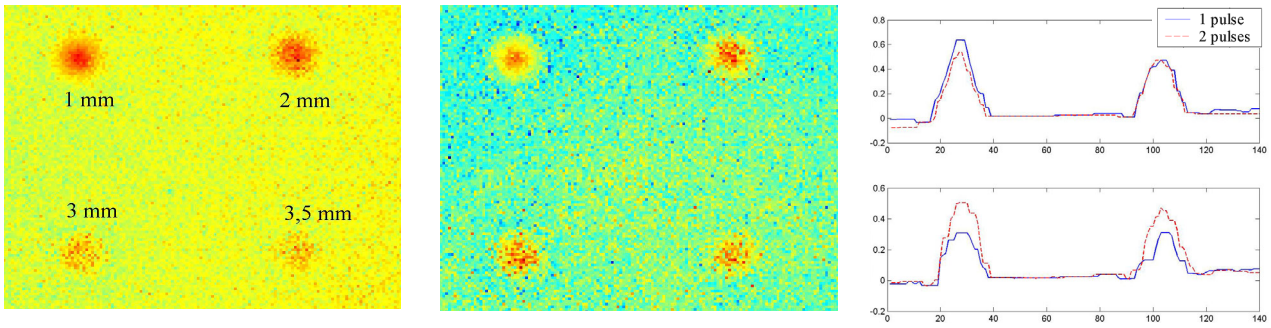

(a) **(b)** **(c)**

Figure 8. Phase images at 1.25 Hz in a mild steel specimen with four defects (a) one Δ duration pulse of amplitude $2A$ (b) 2 pulses of A amplitude separated by δ=3 ms, and (c) corresponding intensity profiles at the center of the four defects.

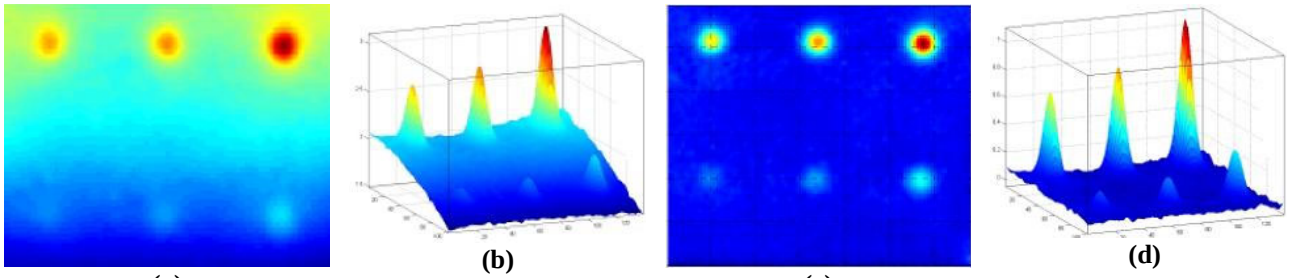

(a) **(b)** **(c)** **(d)**

Figure 9. DAC applied on a Plexiglas™ sample with 6 holes subjected to a strong non-even heating. (a) raw thermogram at 5000 ms, (b) corresponding 3D view. Notice the sharp variation of background intensity values. (c) and (d) are the corrected thermogram after the application of DAC method and its corresponding 3D view, respectively. From [3]

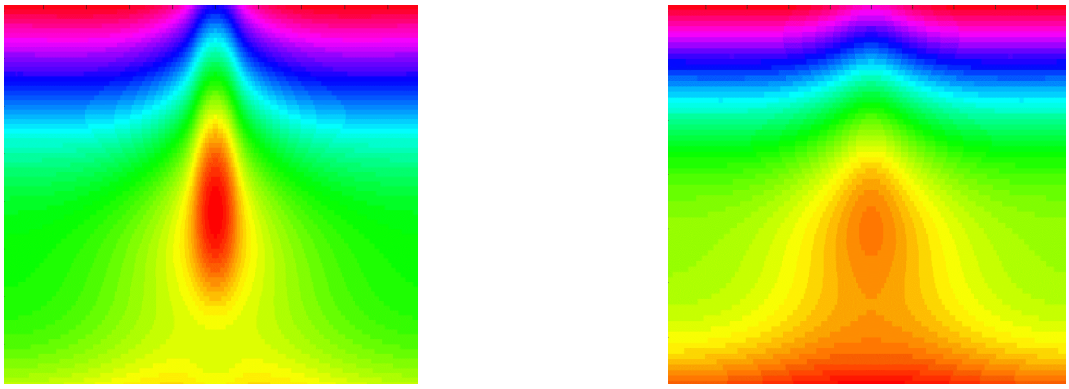

(a) **(b)**

Figure 10. Phase values of the WT for a (a) 1 mm and (b) 3 mm depth defects (flat-bottomed holes in aluminum) as a function of T_r for a line passing over the defect center. ω_0=2 Hz. From [4].